Acta Cryst. (1992). B48, 591–598

Electron Density in Rutile (TiO_2) by the Maximum Entropy Method

BY MAKOTO SAKATA, TATSUYA UNO, MASAKI TAKATA AND RENTARO MORI

Department of Applied Physics, Nagoya University, Nagoya, Japan

(*Received* 31 *January* 1991; *accepted* 5 *February* 1992)

Abstract

The electron-density distribution of rutile, TiO_2, was determined by the maximum entropy method from powder X-ray diffraction data. In the resulting electron-density distribution, the shape of the TiO_2 units on the (001) plane is clearly shown at the 0.4 e Å^{-3} contour level as a consequence of the apical Ti—O bonds of TiO_6 octahedra. TiO_2 units belonging to different layers, *e.g.* those on the (001) and (002) planes, are connected three-dimensionally through the four equatorial Ti—O bonds of the octahedra at the 1.2 e Å^{-3} contour level. However, there is no electron overlap between either Ti—Ti or O—O atoms. From these features, the structure of rutile can be described as TiO_2 'molecules' connected by equatorial Ti—O bonds to form a three-dimensional network. The O atoms, which are believed to have an atomic dipole moment, have a skewed electron density. In contrast to conventional Fourier methods, such details of the electron-density distribution are revealed directly on the electron-density distribution map, not on the deformation map; this visualization of the electron density helps the understanding of the state of the chemical bonding.

1. Introduction

Sakata & Sato (1990) showed that the maximum entropy method (MEM) is a very powerful tool for restoring the detailed information included in structure factors determined accurately by the *Pendellösung* method for Si (Saka & Kato, 1986). Based on this work, Sakata, Mori, Kumazawa, Takata & Toraya (1990) have proposed a new method for obtaining precise electron-density distributions from X-ray powder diffraction data by the use of profile fits and the MEM. In their paper, the electron-density distribution of CeO_2 was shown and an excess of electrons within the oxygen cube was recognized which could be related to the high ionic conductivity of CeO_2. X-ray powder diffraction allows relatively simple measurement of Bragg intensities and is a widely used technique. The benefits that can be obtained by adopting the newly proposed method are great, provided it can be applied to various kinds of materials. It is, therefore, very important to establish the new method by demonstrating its applicability to various substances. In this paper, the results for rutile, TiO_2, are given.

Rutile is one of the substances studied thoroughly by various techniques that were reviewed by Grants (1959). It has one of the best known crystal structures, *i.e.* the rutile structure type. The structure is tetragonal and the space group is $P4_2/mnm$ with a = 4.593659 (18) and c = 2.958682 (8) Å at 298 K (Abrahams & Bernstein, 1971).

The charge density in rutile has been studied by several authors using conventional Fourier methods. Until recently, there had been a long-running discussion concerning the covalency of the bonding in rutile (Baur, 1961; Kingsbury, 1968; Ladd, 1969; Sen, Riga & Verbist, 1976); however, the covalency of the Ti—O bonds has now been established as described in the following. Gronschorek (1982), by multipole refinement from room-temperature data collected using Pd-filtered Ag $K\alpha$ radiation, concluded that bonding in rutile is largely covalent. More recently, Restori, Schwarzenbach & Schneider (1987) have performed an accurate analysis of charge density in rutile by X-ray and γ-ray diffraction and found that there are residual maxima of about 0.3 e Å^{-3} on both types of Ti—O bonds, *i.e.* two long apical bonds of length 1.9800 (9) Å and four short equatorial bonds of length 1.9485 (5) Å, in the static deformation maps. Concerning the physical properties of rutile, Bertaut (1978) found an oxygen dipole moment of 0.78 e Å and predicted a variation of about 0.01 of the oxygen positional parameter between X-ray and neutron diffraction determinations. Very recently, however, Howard, Sabine & Dickson (1991) performed a neutron powder diffraction study on this substance but did not find any significant difference between X-ray and neutron determinations of the oxygen position such as might have resulted from polarization effects. In addition to these reports, Shintani, Sato & Saito (1975) have given a comparison of the charge density of Ti^{4+} (having no d electrons) with that of Ni^{2+} ($3d^8$) in γ-Ni_2SiO_4. The final difference Fourier map for TiO_2 was featureless to within 0.3 e Å^{-3}.

0108-7681/92/050591-08$06.00

One of the reasons for investigating the charge density of rutile is to study the chemical bonding between the Ti and O atoms. In the present method, this can be achieved most straightforwardly by drawing the electron-density distribution itself rather than by resorting to somewhat indirect methods such as drawing the various deformation maps (Restori *et al.*, 1987) or multipole refinement (Gronschorek, 1982). This can make the situation very simple. The purpose of this paper is to investigate whether it is possible to find the weak covalency of the basically ionic crystal directly from the electron-density map.

There are several variations of the MEM. Though the principle of the MEM is the same for all the variations, it is necessary to distinguish between them in some cases. The method used in the present paper is the same as that in Sakata & Sato (1990) and Sakata *et al.* (1990). The unique feature of the method is that it uses no trial density distribution and starts the iteration from a uniform electron-density distribution, *i.e.* the maximum entropy state. In order to emphasize this fact, we call the present method the maximum entropy method with uniform density at the initial stage (abbreviated UDIS or UDIS-MEM). The formalism used in the present method is practically same as that used by Collins (1982). However, the latter method uses a trial density and the final equation was derived with some approximations. Because of this, Collins' method requires that the trial density is close to the final density. It is, however, possible to derive the same equation without any approximation and to use the equation without any trial density. In order to clarify the situation, the theoretical background of the present method is described in the following section.

2. Theory

The information-theoretical entropy, S, is written as

$$S = -\sum\rho'(\mathbf{r})\ln\rho'(\mathbf{r}), \quad (1)$$

where $\rho'(\mathbf{r})$ is the probability density which is related to the actual electron density at a certain pixel $\mathbf{r}$ as

$$\rho'(\mathbf{r}) = \rho(\mathbf{r})/\sum\rho(\mathbf{r}). \quad (2)$$

When the prior probability, $\tau'(\mathbf{r})$, is known

$$\tau'(\mathbf{r}) = \tau(\mathbf{r})/\sum\tau(\mathbf{r}), \quad (3)$$

where $\tau(\mathbf{r})$ is the prior density for $\rho(\mathbf{r})$, the prior-knowledge entropy is written as

$$S = -\sum\rho'(\mathbf{r})\ln[\rho'(\mathbf{r})/\tau'(\mathbf{r})]. \quad (4)$$

As a constraint, we use the following equation

$$C = [1/(N_1 + N_2)][\sum|F_{cal}(\mathbf{k}) - F_{obs}(\mathbf{k})|^2/\sigma^2(\mathbf{k}) + \sum|G_{cal}(j) - G_{obs}(j)|^2/\sigma^2(j)] \quad (5)$$

where N_1 and N_2 are the numbers of observed reflections for nonoverlapped and overlapped peaks, respectively, $F_{obs}(\mathbf{k})$ is the observed structure factor for the reflection $\mathbf{k}$, $\sigma(\mathbf{k})$ is the standard deviation of $F_{obs}(\mathbf{k})$, $F_{cal}(\mathbf{k})$ is the calculated structure factor given as

$$F_{cal}(\mathbf{k}) = V\sum\rho(\mathbf{r})\exp(-2\pi i\mathbf{r}.\mathbf{k}), \quad (6)$$

$G_{obs}(j)$ and $G_{cal}(j)$ are the observed and calculated combined structure factors for jth peak, respectively, and $\sigma(j)$ is the standard deviation for $G_{obs}(j)$. $G_{cal}(j)$ is expressed by the multiplicity of each reflection, $m(\mathbf{k})$, and by $F_{cal}(\mathbf{k})$ as

$$G_{cal}(j) = [\sum m(\mathbf{k})F_{cal}(\mathbf{k})^2/\sum m(\mathbf{k})]^{1/2}. \quad (7)$$

V in equation (6) is the unit-cell volume. Using the Lagrange method of undetermined multipliers, we have

$$Q(\lambda) = -\sum\rho'(\mathbf{r})\ln[\rho'(\mathbf{r})/\tau'(\mathbf{r})] - (\lambda/2)C. \quad (8)$$

Collins (1982) obtained the final equation by setting

$$Q(\lambda)/\rho(\mathbf{r}) = 0. \quad (9)$$

Instead of (9), we introduce the following equation as the maximum condition,

$$Q(\lambda)/\rho'(\mathbf{r}) = 0. \quad (10)$$

By this alteration of the maximum condition, the final equation of the MEM can be derived without any approximation as,

$$\rho(\mathbf{r}) = \exp\{\ln\tau(\mathbf{r}) + (\Lambda/N)\sum[1/\sigma^2(\mathbf{k})] \times [F_{cal}(\mathbf{k}) - F_{obs}(\mathbf{k})]\exp(-2\pi i\mathbf{k}.\mathbf{r}) + \sum[1/\sigma^2(j)G_{cal}(j)\sum m(\mathbf{k})][G_{cal}(j) - G_{obs}(j)] \times \sum m(\mathbf{k})F_{cal}(\mathbf{k})\exp(-2\pi i\mathbf{k}.\mathbf{r})\} \quad (11)$$

where $N = N_1 + N_2$ and $\Lambda = \lambda F_{cal}(0)$. The first two terms of equation (11) are the same as the equation derived by Collins (1982). In order to solve (11), we introduce the zeroth-order single-pixel approximation which replaces (6) by

$$F_{cal}(\mathbf{k}) = V\sum\tau(\mathbf{r})\exp(-2\pi i\mathbf{k}.\mathbf{r}). \quad (6')$$

Using this approximation, all terms on the right-hand side of equation (11) do not depend on $\rho(\mathbf{r})$ and become calculable when the prior distribution is given. In the present method, the uniform density distribution is always used as the initial prior density distribution $\tau(\mathbf{r})$. Since it corresponds to the maximum entropy state in all the possible density distributions, we can exclude any prejudice in the process of choosing the prior density distribution. Once the initial prior distribution has been chosen, equation (11) may be solved iteratively (Sakata & Sato, 1990). It is known that the final results of an MEM deduction do not depend on the choice of the value of λ (Gull & Daniel, 1978; Sakata & Sato, 1990),

since once a set of data, $F_{obs}(\mathbf{k})$ and $\sigma(\mathbf{k})$ is given, there is no room in UDIS-MEM for any prejudice to be introduced in calculating the MEM map.

3. Experimental

The specimen used in the present work was a NIST intensity standard like the CeO_2 powder used in the previous paper (Sakata *et al.*, 1990). It is important to use a randomly oriented powder specimen, to allow details of the electron-density distribution to be observed. The specimen was therefore first examined by electron microscopy. A transmission electron micrograph of the sample is shown in Fig. 1. The typical particle size was about 0.2 μm. The specimen was also examined by observing an ω-scan profile (Fig. 2). Both examinations gave results that are very similar to those for the CeO_2 powder specimen. Therefore, it was confirmed that the present specimen is as good as the CeO_2 powder for X-ray powder diffraction as far as the particle distribution is concerned.

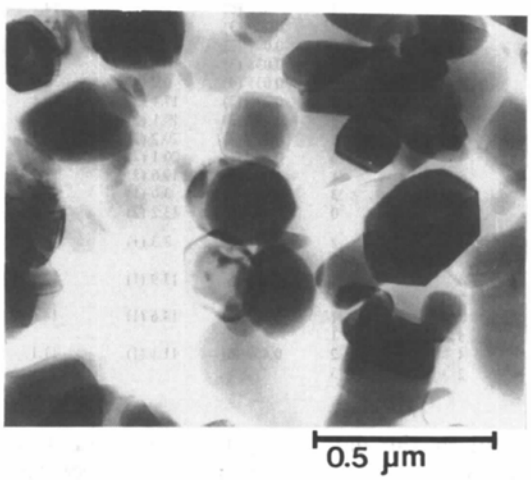

Fig. 1. Transmission electron micrograph of the TiO_2 powder specimen.

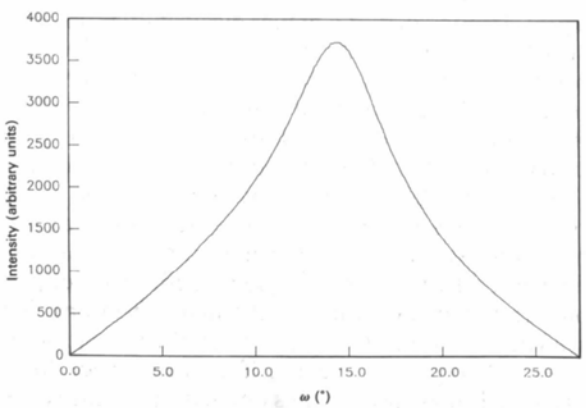

Fig. 2. An ω-scan profile for the TiO_2 powder specimen.

The powder X-ray diffraction experiment was performed using a two-axis diffractometer attached to a Rigaku 300 mA X-ray generator. Cu $K\alpha$ radiation monochromatized by PG(002) was used as the incident X-ray. No attempt was made to separate Cu $K\alpha_1$ and Cu $K\alpha_2$ radiation. The X-ray powder patterns were recorded in steps of 0.02° in 2θ, and the counting time at each point was 100 s. The scan range was from 23 to 146° and the maximum intensity recorded was 360 714 counts at 27.40° in 2θ. It took approximately 7 days to complete the whole scan (a whole powder pattern would take extraordinarily long at this rate). The reason for such a long scan is to collect the most reliable intensity data to reveal the detailed electron-density distribution. It was, however, found that the sample contained a small amount of impurity which was identified as a phase of the TiO_2 polymorph anatase. In the present case these impurity peaks could be detected because of the extraordinarily long scan. Since most of impurity peaks were isolated or weak, virtually no problems arose from the contamination by anatase. An exception is the overlapping of rutile (211) with anatase (105) and (211) reflections. In order to show the degree of disturbance by the overlapping of these peaks and estimate the accurate integrated intensity of rutile (211), the observed profile intensities for these peaks are plotted in Fig. 3. At a glance, the existence of anatase peaks in Fig. 3(*a*) may not be recognized. It is, therefore, clear that the contamination of anatase is not very significant. In the present analysis, however, it is important to estimate the integrated intensities as accurately as possible. We tried to eliminate the contribution of the anatase phase to the rutile (211) reflection by using a profile-fitting technique. The results of profile fitting are shown in Fig. 3(*b*).

After careful examination of all rutile peaks and profile fitting, the integrated intensities and their standard errors were obtained from the powder pattern (Table 1). The errors were estimated by the least-squares refinement of profile fits (Toraya, 1986) and not from the formula, $\sqrt{I}$, which is often used for the estimation of statistical error. As is usual, the overall difference between the observed and the calculated intensities obtained by profile fitting is smaller than that of the Reitveld refinement, since the profile-fitting analysis is free from the restrictions of the structural model used in the Rietveld refinement.

The observed integrated intensities were converted to structure factors by using the scale factor determined by a least-squares analysis in which Lorentz and polarization factors, Lp, were con-

sidered to be given by

$$\mathrm{Lp} = (1+\cos^2 2\theta \cos^2 2\theta_M)/\sin 2\theta \cos\theta \qquad (12)$$

where θ_M is Bragg angle of a monochromator used in the experiment. The structure-factor data and their standard deviations used in the subsequent MEM analysis are included in Table 1. The whole process of data analysis is also described in Sakata *et al.* (1990).

4. MEM density map

The computer program used by Sakata *et al.* (1990) was modified for the space group of TiO_2, *i.e.* $P4_2/mnm$. By using the F_{obs} data in Table 1, the electron-density distribution of TiO_2 (rutile) was obtained by the UDIS-MEM. It will be called an MEM density map in this paper. The number of pixels used in the calculation was $64 \times 64 \times 64$ and 350 iterations were needed to satisfy the convergence criterion, $C \leq 1$.

In Fig. 4, the MEM density map of the (002) plane is shown. In UDIS-MEM, no structural model is assumed in the data analysis. After obtaining the MEM density map, therefore, it is necessary to assign the density peaks to the constituent atoms or ions. This can be achieved very easily from the number of electrons in the peaks. In the present case, the Ti and O ions were assigned as shown in the figure. In Fig. 4(*a*), the higher electron-density region between 5.0 and 50.0 e $Å^{-3}$ is shown with 5.0 e $Å^{-3}$ contour steps. In the figure, the inner electrons of Ti core must be still omitted but it can be noticed that the electron-density distribution of Ti is very isotropic. For the O ions, all the core electrons are fully shown. It can be seen from the figure that the oxygen core electrons are skewed. One possibility is to attribute this skewness to anharmonic thermal vibration (neutron diffraction would give a definite description on the anharmonicities of thermal vibration). This skewness must be considered when the atomic polarization of oxygen is argued, if oxygen nuclei do not show such skewness. In this context, it would be very interesting to analyze the neutron diffraction data by

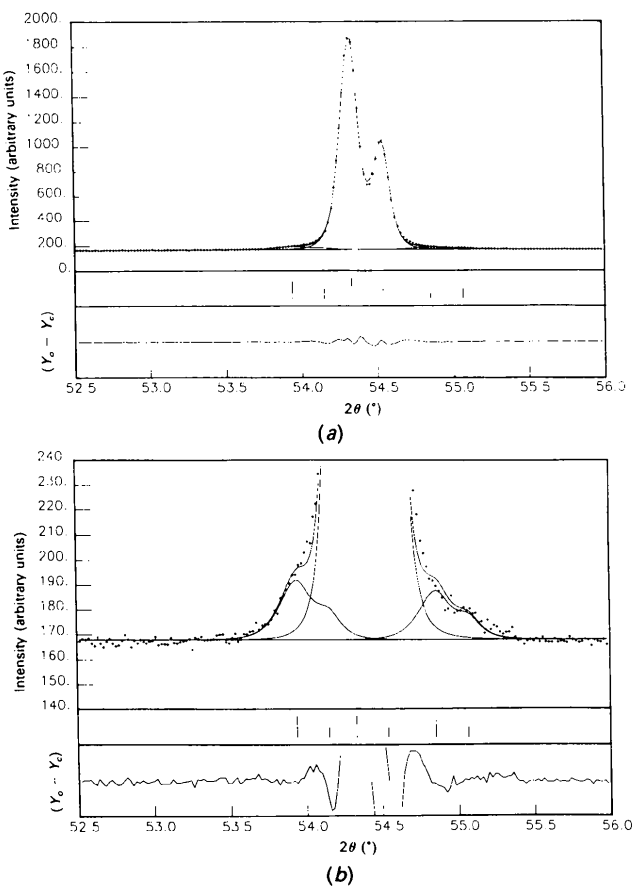

Fig. 3. Results of profile fitting for (211) reflections from TiO_2. (*a*) and (*b*) are plotted on different intensity scales.

Table 1. *The observed integrated intensity, I_{obs}, the observed structure factor, F_{obs}, and the calculated structure factor from the MEM map, F_{MEM}, for each peak*

The observed structure factor was obtained from I_{obs} using the scale factor and the phase was calculated from the rutile structure.

h	k	l	I_{obs}	F_{obs}	F_{MEM}
1	1	0	6.84 (2)	38.5 (3)	37.4
1	0	1	2.91 (1)	23.7 (2)	23.8
2	0	0	0.404 (3)	13.7 (1)	13.8
1	1	1	1.395 (6)	−19.0 (2)	−18.8
2	1	0	0.518 (3)	12.4 (1)	12.4
2	1	1	4.02 (1)	30.8 (3)	29.9
2	2	0	1.250 (6)	35.9 (3)	35.7
0	0	2	0.540 (2)	37.2 (3)	37.2
3	1	0	0.565 (2)	19.4 (2)	19.4
2	2	1	0.048 (2)	5.8 (1)	−5.8
3	0	1	1.387 (6)	32.8 (3)	33.2
1	1	2	0.696 (6)	23.5 (3)	23.6
3	1	1	0.075 (3)	5.7 (1)	5.7
3	2	0	0.015 (1)	−3.6 (2)	−3.7
2	0	2	0.158 (4)	12.1 (1)	12.1
2	1	2	0.074 (2)	6.1 (1)	6.1
3	2	1	0.309 (5)	12.7 (1)	12.6
4	0	0	0.196 (4)	20.5 (2)	20.8
4	1	0	0.080 (7)	−9.4 (4)	−9.4
2	2	2	0.490 (4)	23.6 (2)	23.8
3	3	0	0.265 (4)	24.7 (3)	24.9
4	1	1	0.466 (6)	16.6 (2)	16.7
3	1	2	0.366 (6)	14.7 (1)	14.7
4	2	0	0.209 (3)	15.8 (2)	15.9
4	2	1	0.047 (2)	5.2 (1)	5.3
1	1	3	0.038 (3)	−6.6 (3)	−6.8
4	3	0	0.035 (4)	6.2 (4)	6.0
4	0	2	0.275 (2)	17.1 (2)	17.1
5	1	0	0.348 (3)	19.1 (2)	18.8
3	3	2	0.429 (3)	20.2 (2)	20.1
3	0	3	0.56 (1)	20.1 (2)	20.2
5	2	1	1.095 (4)	19.0 (2)	18.9
3	1	3	0.029 (3)	3.0 (1)	3.0
4	4	0	0.145 (3)	13.2 (2)	13.2
3	2	2	0.178 (4)	8.3 (1)	8.4
1	0	3			
4	1	2	0.769 (5)	13.9 (1)	13.7
2	1	3			
4	3	1	0.664 (3)	14.6 (1)	14.6
5	0	1			
4	2	2	0.459 (6)	11.1 (1)	11.1
2	2	3			

the MEM. As for the skewness, this will be discussed in detail later.

In Fig. 4(*b*), the lower electron-density region is shown from 0.4 to 5.0 e $Å^{-3}$ with 0.4 e $Å^{-3}$ steps. For convenience, the MEM map for four unit cells is shown in Fig. 4(*b*). It can clearly be seen that rutile is not a simple ionic crystal but has a TiO_2 molecule-like unit on this plane formed by apical bonds at the 0.4 e $Å^{-3}$ level. Additionally, the anisotropies of the electron-density distributions for both Ti and O ions are very remarkable at the lower-density level. It is not appropriate, however, to interpret these anisotropies as anisotropic thermal vibrations. Here again a neutron diffraction experiment would give a definite answer. It looks as if TiO_2 molecules float in the space on this plane. Although we checked the density level less than 0.4 e $Å^{-3}$, there is no trace suggesting nearest neighbor O—O bonds. The molecule-like units are not connected with each other on the (001) plane.

In Fig. 5, the MEM density map of the (110) plane is shown. It can be seen from the figure that the TiO_2 molecule-like units are not isolated nor weakly bound by van der Waals forces, but are connected by equatorial Ti—O bonding on the (110) plane at the 1.2 e $Å^{-3}$ level. Judging from the overlapped electron clouds, the bonding force of the equatorial Ti—O bonds is stronger than that of the apical Ti—O bonds. Considering the fact that the apical bonds are longer than the equatorial bonds [1.9800 (9) and 1.9485 (5) Å, respectively] (Restori *et al.*, 1987), these results seem to be very reasonable. In contrast to CeO_2, there are no excess electrons in any vacant site.

It is adequate therefore to describe the fine structure of rutile in the crystalline state as consisting of TiO_2 molecule-like units formed on the (100) and (200) planes and connected three-dimensionally through equatorial Ti—O bonds which are slightly stronger than the apical Ti—O bonds. The three-dimensional network structure of rutile, which is directly observed in the present analysis, is shown schematically in Fig. 6. These results are very reasonable for the chemical bonding of rutile. It should be pointed out that the skewness of the oxygen core electrons can also be seen in Fig. 5(*a*), while the electron-density distribution of Ti core electrons is again isotropic on the (110) plane. The skewness in Fig. 5(*a*) seems to be greater than that in Fig. 4(*a*).

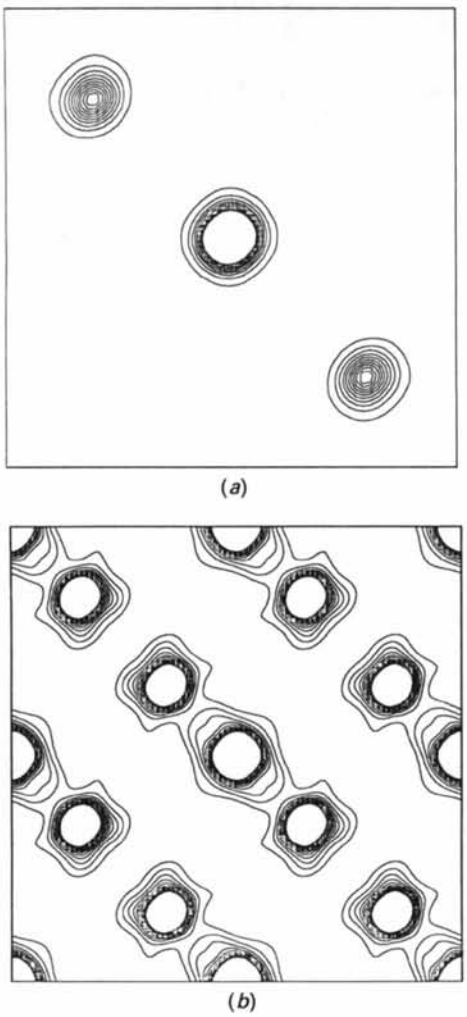

Fig. 4. MEM map of the TiO_2 (002) plane: (*a*) higher- and (*b*) lower-density region. The contour levels are indicated in the text.

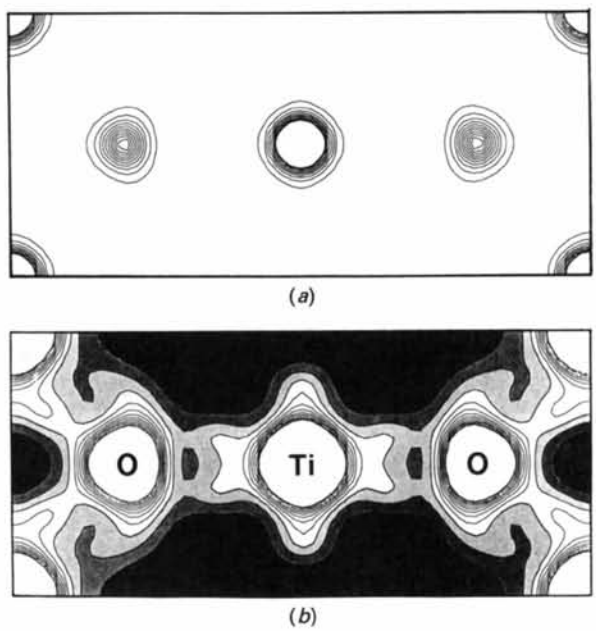

Fig. 5. MEM map of the TiO_2 (110) plane: (*a*) higher- and (*b*) lower-density region. Contour levels are the same as in Fig. 4.

In order to confirm the results described above, we performed the same experiment and analysis independently with a shorter collection time. The counting time was 20 s at each point. In profile fitting, the contamination by the anatase phase was ignored because of the lower number of intensity statistics. Despite the use of less reliable data, basically the same results were obtained. The main difference was in the shape of the contour line at lower levels, such as at 0.4 e $Å^{-3}$.

5. Calculated structure factors from the MEM map

In the work of Restori *et al.* (1987), the structure factors were determined very accurately. The data were analyzed by conventional methods and the charge density in rutile was thoroughly studied by the difference Fourier method. It would be interesting to compare the results obtained by conventional and present methods. The comparison could be made either in real space or reciprocal space. It is, however, not practically possible to calculate the MEM map by using all the data of Restori *et al.* because of the time and cost of the computation for the large structure-factor data set. Hence the comparison will be made in the form of structure factors. First some structure factors are listed in Table 2, which are measured by three different experimental techniques: powder X-ray diffraction (present work), and γ-ray and single-crystal X-ray diffraction (Restori *et al.*, 1987). For the single-crystal X-ray data, the extinction-corrected values were not available. Owing to extinction effects, the single-crystal X-ray data are considerably smaller than the other data sets but the independently measured powder X-ray data and the γ-ray data agree very well with each other. Restori *et al.* (1987) performed γ-ray diffraction to determine the scale factor experimentally, which enabled the structure factors to be measured on an absolute scale. Although the powder X-ray data were not measured on an absolute scale, it can be said that their reliability is high.

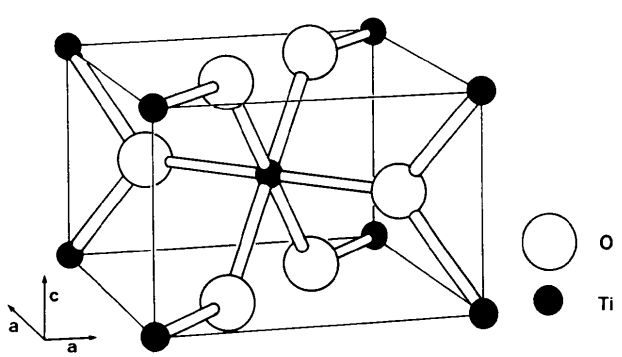

Fig. 6. Schematic drawing of the TiO_2 network.

Table 2. *Observed structure factors from powder X-ray, F_{obs}, γ-ray, $F(\gamma)$, and single-crystal X-ray diffraction, F_o*

h	k	l	F_{obs}	$F(\gamma)$	F_o
0	0	2	37.2	37.69	33.0
3	0	1	32.8	31.97	29.2
1	0	1	23.7	23.44	21.7
4	0	0	20.8	19.79	19.4

The number of structure factors measured in the present experiment (Table 1) is very limited. Overall, 34 structure factors were obtained individually by the profile-fitting method and four combined structure factors were measured. In the conventional Fourier method, the limited number of data would cause very severe Fourier-series termination effects. A few examples can be seen in Sakata & Sato (1990) and Sakata *et al.* (1990). In the maximum entropy method, however, the limitation of the number of data does not always cause significant errors in the electron density map, because the maximum entropy method deduces the values of structure factors for unmeasured reflections. In order to demonstrate this fact in the case of rutile, structure factors which were not measured in the present experiment were calculated from the MEM density map. In Table 3, the calculated structure factors from the MEM map, F_{cal}, are listed together with the observed structure factors, F_o, obtained by Restori *et al.* (1987) using a single crystal in the d-spacing range 0.788–0.637 Å, which covers the lowest 40 unmeasured structure factors in the present powder experiment. The phases of F_{cal} and F_o coincide exactly with each other in all cases and hence only the absolute values are given in Table 3. In this region, the effect of extinction on the single-crystal data must be very small. If the overall agreement is expressed by an R factor or a weighted R factor, it gives $R = 0.082$ or $wR = 0.086$. It is not easy to say whether an 8% level of agreement is good or not. Considering the fact that there are no adjustable parameters in the present analysis, it would be appropriate to mention that the MEM map has the ability to predict the unmeasured data, and hence can partially compensate for the limited number of powder diffraction data. Such an ability of the maximum entropy method should be thoroughly studied from the various viewpoints.

6. Discussion

By UDIS-MEM using X-ray powder diffraction data, we have analyzed both ceria (CeO_2) and rutile (TiO_2) in the previous and present works, respectively. Both are basically ionic crystals. UDIS-MEM has been successful in revealing the differences in the bonding nature of these substances from the obser-

Table 3. *Calculated values of unmeasured structure factors in the present powder experiment from the MEM map, F_{cal}, and the observed single-crystal structure factors from Restori et al.* (1987), F_o

h	k	l	$\|F_{cal}\|$	$\|F_o\|$
5	3	0	7.76	7.11
4	4	1	4.46	5.80
4	3	2	2.96	3.07
3	2	3	9.21	8.61
5	1	2	14.38	14.08
6	0	0	15.37	14.57
5	3	1	0.11	0.68
6	1	0	5.06	4.69
0	0	4	17.02	18.02
5	2	2	0.12	0.48
4	1	3	11.27	11.41
6	1	1	11.33	10.55
3	3	3	0.25	1.26
6	2	0	9.82	9.00
1	1	4	12.16	12.53
5	4	0	0.54	0.92
4	4	2	10.58	11.04
4	2	3	3.47	3.35
6	2	1	2.70	3.02
2	0	4	7.78	7.43
5	4	1	9.15	9.84
2	1	4	3.14	3.28
5	3	2	6.87	6.38
6	3	0	1.57	2.08
6	0	2	11.85	13.03
2	2	4	12.44	14.14
6	1	2	3.52	4.20
5	0	3	5.67	5.67
4	3	3	10.76	11.68
6	3	1	10.72	12.08
5	1	3	0.66	0.74
3	1	4	8.76	9.39
6	2	2	8.04	8.19
5	5	0	12.68	14.49
7	1	0	8.46	8.68
5	4	2	0.62	0.76
5	2	3	11.76	13.82
7	0	1	11.97	12.87
3	2	4	1.23	1.70
6	4	0	9.79	10.39

vation of the detailed electron-density distribution, that is, the existence of excess electrons in ceria and the three-dimensional network structure in rutile. These fine structures are very reasonable features, judging from the physical properities of these substances. It is, therefore, understood that UDIS-MEM is a very powerful tool for observing fine details of structures which can be closely related to the physical and/or chemical properties of the various materials.

Concerning the high static dielectric constant of rutile (Parker, 1961), the oxygen polarizability has been discussed in several papers. Kingsbury (1968) and Bertaut (1978) suggested a rather high dipole moment for the oxygen ions, about 0.8 e Å, from the difference between the value for the oxygen position parameter determined by X-ray and neutron diffraction. Very recently, Howard *et al.* (1991) have, based on newly determined values, questioned the high polarizability of oxygen ions and noted that the difference of oxygen positional parameter is two orders of magnitude less than that suggested by Kingsbury (1968) or Bertaut (1978). These discussions are based on the displacement of the central position of the electron cloud (negative charge) from nucleus (positive charge). By applying UDIS-MEM to both neutron and X-ray diffraction data, the distribution of the positive and negative charge can be obtained and the atomic polarization of oxygen ions can be treated more precisely. In this context, the skewness of the electron density of the oxygen ions shown in Figs. 4(*a*) and 4(*b*) may have an important consequence. It would be very interesting to investigate by neutron diffraction whether or not the skewness of the positive charge distribution exists.

It is very well known that electron-density distribution maps obtained by Fourier summation suffer from truncation effects of the Fourier coefficients. When the number of Fourier coefficients is limited such as in the case of powder diffraction, truncation effects become very severe. In order to minimize truncation effects, it is usual to draw a difference Fourier map, in which differences of Fourier coefficients between observed and calculated structure factors are used. The calculated structure factors are obtained by using a certain structural model. This implies the setting of unobserved structure factors to be equal to the calculated structure factors from that model. It is possible to draw various difference Fourier maps by changing structural models. From the viewpoint of the MEM analysis, this is equivalent to changing the estimation of unobserved structure factors. On the other hand, the electron-density distribution is obtained directly without assuming any structural models in the MEM analysis. This means that unobserved structure factors are estimated without any prejudice, and this can be a big advantage of the MEM analysis over conventional methods.

In UDIS-MEM, an electron-density distribution (MEM map) is obtained for a given data set, which is the least biased with respect to the missing information. It is, however, very difficult to tell whether we can believe all the details of the MEM map. It all depends on the number of data used in the MEM analysis and on their accuracies. In other words, an MEM map is also dependent on resolution, since the number of structure-factor data is finite and each datum has an error. It can, however, be said from the results which have been already analyzed by the MEM that the MEM density map covers a wide range of electron densities which should be trusted. In other words, the dynamic range of the MEM map is very high compared with the density map obtained by conventional Fourier summation. The details of electron density are usually described by deformation maps in conventional methods and it is possible to draw many different deformation maps by changing the structural model to be subtracted. Indeed, Restori *et al.* (1987) showed six different deformation maps. Some unnecessary

complexities can be introduced by this fact, since it is not always clear which deformation map should be trusted. For example, deformation densities near Ti- and O-ion sites are rather different depending on the structural model subtracted. It is also not clear from these deformation maps which Ti—O bond is stronger, the two long apical bonds or the four short equatorial bonds, since deformation densities of two bonds were reversed depending on the model. It cannot be avoided that the information obtained from deformation maps is somewhat indirect compared with that of an MEM map.

7. Concluding remarks

The electron-density distribution in TiO_2 (rutile) has been obtained from X-ray powder diffraction data by analyzing the UDIS-MEM. The MEM map reveals not only the basic rutile structure but also a three-dimensional network structure consisting of TiO_2 'molecules'. It also demonstrated the skewness of the oxygen core electron-density distribution, which may be affected by the atomic polarization of oxygen. The present work again proved that the UDIS-MEM is a very powerful method for visualizing the details of the electron-density distribution. In order to interpret the 'observed' electron density, however, an analysis of both X-ray and neutron diffraction data for the same material is required. Such a study would provide a concrete answer as to whether the deformation of the electron density results from the lattice or the electron system. Through such studies, new aspects of crystallography may be developed.

The authors thank the Computer Center, Institute for Molecular Science, Okazaki National Research Institutes, for the use of the HITAC M-680H and S-820/80 computers and the library program *ABCXYZ* written by T. Yamada (IMS). A part of the computations in this work were also carried out at the Computer Center of Nagoya University which is gratefully acknowledged by the authors. This work has been partly supported by a Grant-in-Aid for Scientific Research from the Ministry of Education, Science and Culture.

References

ABRAHAMS, S. C. & BERNSTEIN, J. L. (1971). *J. Chem. Phys.* **55**, 3206–3211.
BAUR, W. H. (1961). *Acta Cryst.* **14**, 209–213.
BERTAUT, E. F. (1978). *J. Phys. (Paris)*, **39**, 1331–1347.
COLLINS, D. M. (1982). *Nature (London)*, **298**, 49–51.
GRANTS, F. A. (1959). *Rev. Mod. Phys.* **31**, 646–674.
GRONSCHOREK, W. (1982). *Z. Kristallogr.* **160**, 187–203.
GULL, S. F. & DANIEL, G. J. (1978). *Nature (London)*, **272**, 686–690.
HOWARD, C. J., SABINE, T. M. & DICKSON, F. (1991). *Acta Cryst.* B**47**, 462–468.
KINGSBURY, P. I. (1968). *Acta Cryst.* A**24**, 578–579.
LADD, M. F. C. (1969). *Acta Cryst.* A**25**, 486–487.
PARKER, R. A. (1961). *Phys. Rev.* **124**, 1719–1722.
RESTORI, R., SCHWARZENBACH, D. & SCHNEIDER, J. R. (1987). *Acta Cryst.* B**43**, 251–257.
SAKA, T. & KATO, N. (1986). *Acta Cryst.* A**42**, 469–478.
SAKATA, M., MORI, R., KUMAZAWA, S., TAKATA, M. & TORAYA, H. (1990). *J. Appl. Cryst.* **23**, 526–534.
SAKATA, M. & SATO, M. (1990). *Acta Cryst.* A**46**, 263–270.
SEN, S. K., RIGA, J. & VERBIST, J. (1976). *Chem. Phys. Lett.* **39**, 560–564.
SHINTANI, H., SATO, S. & SAITO, Y. (1975). *Acta Cryst.* B**31**, 1981–1982.
TORAYA, H. (1986). *J. Appl. Cryst.* **19**, 440–447.

Acta Cryst. (1992). B**48**, 598–604

Structures and Electron Density Distributions of $[Cl—P(NPCl_3)_3]^+.Cl^-$ and $[Cl—P(NPCl_3)_3]^+.PCl_6^-.\frac{1}{2}C_2H_2Cl_4$ at 100 K

BY FERDINAND BELAJ

Institut für Anorganische Chemie der Karl-Franzens-Universität Graz, Schubertstraße 1, A-8010 Graz, Austria

(*Received* 27 *November* 1991; *accepted* 26 *March* 1992)

Abstract

Chlorotris(trichlorophosphazeno)phosphonium chloride (1), $Cl_{11}N_3P_4$, $M_r = 555.9$, trigonal, $R3$, $a = 10.600$ (1), $c = 14.167$ (2) Å, $V = 1378.5$ (3) Å^3, $Z = 3$, $D_x = 2.009$ Mg m^{-3}, λ(Mo $K\alpha$) = 0.71069 Å, $\mu = 2.00$ mm^{-1}, $F(000) = 804$, $T = 100$ K, $R = 3.10$, $wR = 2.91\%$ for 1981 unique observed reflections and 54 parameters. Chlorotris(trichlorophosphazeno)phosphonium hexachlorophosphate–1,1,2,2-tetrachloroethane (2/1) (2), $Cl_{16}N_3P_5.\frac{1}{2}C_2H_2Cl_4$, $M_r = 848.1$, orthorhombic, $Cmca$, $a = 21.627$ (7), $b = 16.106$ (3), $c = 14.899$ (2) Å, $V = 5189.7$ (8) Å^3, $Z = 8$, $D_x = 2.171$ Mg m^{-3}, λ(Mo $K\alpha$) = 0.71069 Å, $\mu =$

0108-7681/92/050598-07$06.00